frontiers in Physics

BRIEF RESEARCH REPORT
published: 17 March 2022
doi: 10.3389/fphy.2022.845958

Applications of Multi-Contrast Optical Coherence Tomography in Assessment of Dysplastic Nevi to Malignant Melanoma

Pei-Yu Lai[1], *Tai-Yu Shih*[1], *Chung-Hsing Chang*[2,3,4]* *and Wen-Chuan Kuo*[1]*

[1]*Institute of Biophotonics, National Yang Ming Chiao Tung University, Hsinchu, Taiwan,* [2]*Skin Institute, Hualien Tzu Chi Hospital, Buddhist Tzu Chi Medical Foundation, Hualien, Taiwan,* [3]*Doctoral Degree Program in Translational Medicine, Tzu Chi University and Academia Sinica, Hualien, Taiwan,* [4]*Institute of Medical Sciences, Tzu Chi University, Hualien, Taiwan*

Melanoma is fatal for skin cancer. One of the essential predictive points in melanoma progression is the development of dysplastic nevi. This study observes subcutaneous blood vessels, lymphatic vessels, and skin thickness in a mouse model of dysplastic nevi *in vivo* through noninvasive, high-resolution, and multi-contrast optical coherence tomography (MCOCT). The subcutaneous microenvironment of the mice showed increased density of lymphatic vessels, dilated walls, and increased thickness of ears during the change of dysplastic nevi; and fragmentation of blood vessels at the later stage of the experimental period. Compared with conventional OCT only provides structure anatomy, MCOCT provides more extensive information for disease analysis and has the potential to detect progressive changes in dysplastic nevi.

Keywords: early detection, multi-contrast, optical coherence tomogaphy, dysplastic nevi, melanoma

OPEN ACCESS

Edited by:
Guan-Yu Zhuo,
China Medical University, Taiwan

Reviewed by:
Xiaojun Yu,
Northwestern Polytechnical University, China
Ramy Abdlaty,
McMaster University, Canada

***Correspondence:**
Chung-Hsing Chang
miriamchangch@gmail.com
Wen-Chuan Kuo
kuo@nycu.edu.tw

Specialty section:
This article was submitted to Optics and Photonics, a section of the journal Frontiers in Physics

Received: *30 December 2021*
Accepted: *11 February 2022*
Published: *17 March 2022*

Citation:
Lai P-Y, Shih T-Y, Chang C-H and Kuo W-C (2022) Applications of Multi-Contrast Optical Coherence Tomography in Assessment of Dysplastic Nevi to Malignant Melanoma. Front. Phys. 10:845958. doi: 10.3389/fphy.2022.845958

INTRODUCTION

Melanoma is the least common and most deadly of all skin cancers. To reduce mortality, early detection of patients with potentially highly metastatic melanoma is the primary modality for surgical excision or targeted therapy [1]. Melanoma is caused by skin cells that begin to develop abnormally. Exposure to ultraviolet light from the sun is thought to cause most melanomas. However, there is evidence suggesting that some melanoma formation is known to be associated with mutations in several primary oncogenes, which transform melanocytes into benign melanotic nevi with histological features such as dysplastic nevi [2,3]. Moreover, David E Elder [4] describes the clinical symptoms of dysplastic nevi and its association with melanoma.

Dysplasia nevi are characterized by clinically atypical and histological structural disorders and cell abnormalities. They are defined histologically and clinically as benign melanocyte-formed moles, and these moles contain the same genes as those in melanoma mutations such as v-Raf murine sarcoma viral oncogene homolog B1 (BRAF) and neuroblastoma RAS viral oncogene homolog (NRAS). Thus, dysplastic nevi are often used as a marker for increased risk of melanoma in the clinical setting. The progression of nevi is usually arrested by various tumor suppressor mechanisms, such as growth arrest regulated by *Pten* protein in the mitogen-activated protein kinase (MAPK) cell messaging pathway. However, these melanocytic nevi may progress to melanoma with a high mortality rate if mutations in genes in the tumor suppressor mechanism, result in the inactivation of specific proteins. In addition, vascular endothelial growth factor (VEGF) has been found to be released by tumor cells. The binding of VEGF to receptors in the lymphatic vessels and vascular endothelium promotes

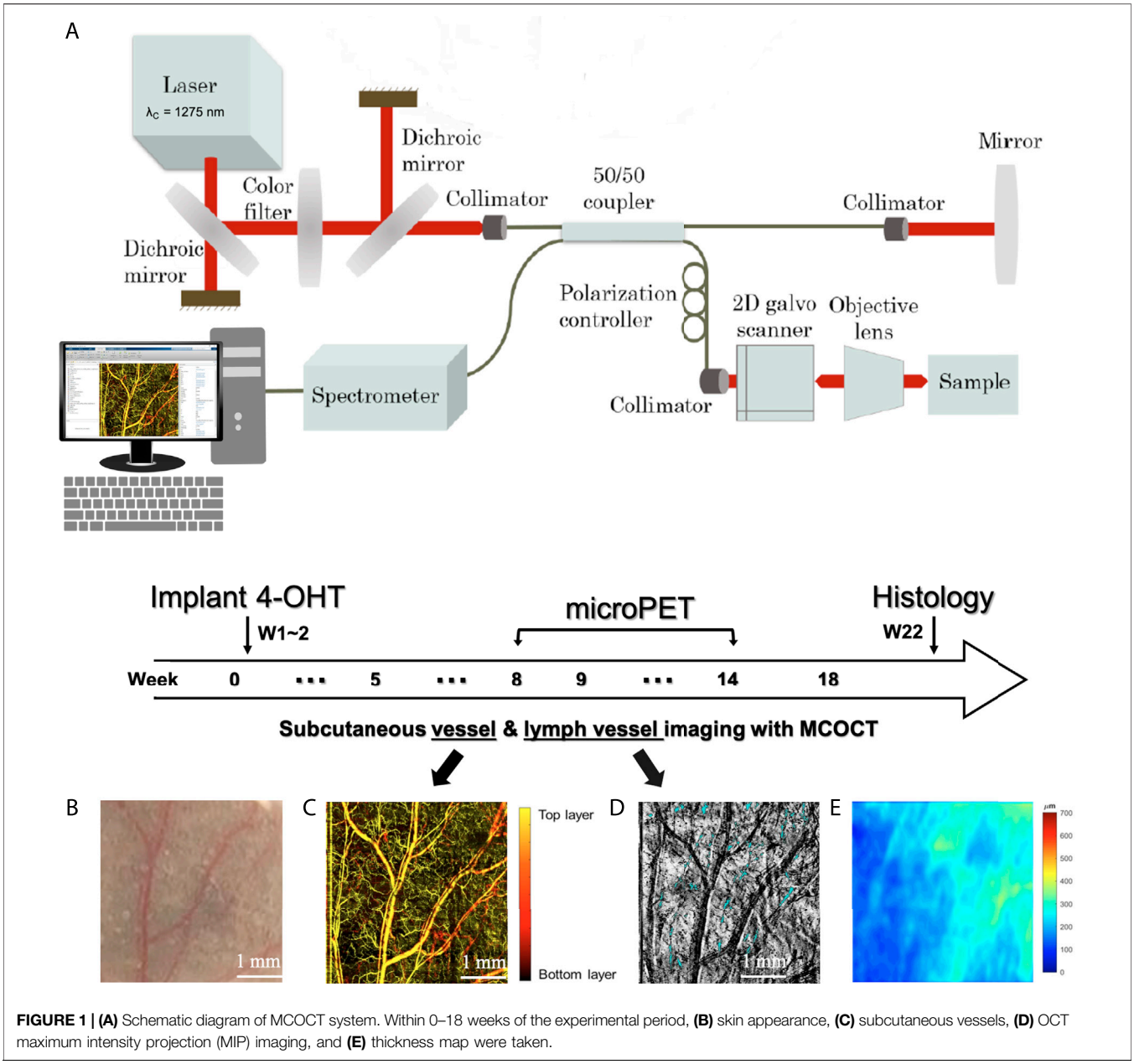

FIGURE 1 | (A) Schematic diagram of MCOCT system. Within 0–18 weeks of the experimental period, **(B)** skin appearance, **(C)** subcutaneous vessels, **(D)** OCT maximum intensity projection (MIP) imaging, and **(E)** thickness map were taken.

lymphatic vessel neogenesis [5–7] and angiogenesis [8–10]. These make vascular and lymphatic vessel changes an important entry point for melanoma research. Therefore, in the study of melanoma and other diseases, invasive methods such as injecting fluorescent markers to mark blood vessels [11] and lymphatic vessels [12] or using immunostaining sections [13] have been used in the past, which may cause side effects such as pain and anxiety to the patients. Therefore, noninvasive imaging systems are increasingly used in cancer research and clinical care [14–17].

Currently, noninvasive diagnostic tools commonly used for skin cancer diagnosis include reflected confocal microscopy (RCM), high-frequency ultrasonography, hyperspectral imaging (HSI), diffuse reflectance spectroscopy (DRS) and optical coherence tomography (OCT) [18–24]. The resolution of RCM is about 1 μm, and the penetration depth is limited by about 200 μm. The resolution of high-frequency ultrasonography can reach 80–200 μm depending on the center frequency. OCT has the advantage of high penetration depth compared with RCM and high resolution compared with high-frequency ultrasound scanning. The OCT technique was initially meant for imaging human retinas and has become a critical diagnostic technology in ocular diseases. The advances of fast and high-resolution OCT instruments during the past 10 years have opened new fields of

applications and perspectives for further development of OCT imaging [25–27]. Thus, OCT has become an evolving imaging technology in the field of oncology due to its noninvasive, real-time two-dimension (2D) and three-dimension (3D) imaging capability with high-resolution (10–20 μm) and adequate depth of 1.5–2 mm without contrast agent and radiation. The images can be compared to corresponding histopathological sections and are potential for early cancer detection, differentiation, and screening or monitoring cancer therapy. Moreover, functional extension of OCT combines the advantages of OCT with additional image contrast obtained by using the Doppler flow, spectroscopy, or polarization as a contrast source [28–30].

Therefore, in this study, we used a multi-contrast OCT (MCOCT), including conventional intensity OCT and functional extension of OCT (i.e., OCT angiography and lymphangiography), into skin cancer study, mainly focused on the study of nevus-to-melanoma transition in a dysplastic nevi mouse model. Furthermore, we longitudinally monitored the micro-environmental changes in the skin during the progression from dysplastic nevus to melanoma by using the noninvasive features of the MCOCT to obtain angiographic, lymphatic vascular, and thickness information, to improve the accuracy of melanoma diagnosis.

MATERIALS AND METHODS

Figure 1A shows a schematic diagram of the MCOCT system. The MCOCT system was developed in-house [31], where the light source has a central wavelength of 1,275 nm and a spectral bandwidth of 240 nm, delivering the axial resolution of ~ 5 μm in the air. A 3D data set consists of 400 steps and covers the image volume of 4*4*2 mm^3. The ear thickness was measured as the distance between the corneum stratum and the articular cartilage in each 2D cross-sectional image. The top boundary and dermis-cartilage junction were determined using the method described in the literature [32]. Therefore, operator-dependence manual boundary-determined steps were not necessary. The enface angiography and lymphangiography were obtained using the optical microangiography algorithm [33] and lymphatic segmentation algorithm [32], respectively. During the acquisition of MCOCT images, the mouse was anesthetized using 1% isoflurane, and the ear was fixed on the stage using double-sided tape. All animal procedures were reviewed and approved by the Institutional Animal Care and Use Committee (IACUC) of National Yang Ming Chiao Tung University, where these experiments were performed.

$BRAF^{V600E}$ induced and *Pten*-deficient metastatic melanoma mouse model was used in this study [34]. Mice were treated topically on the ear with 4-Hydroxytamoxifen (4-OHT) to elicit $BRAF^{V600E}$ and silence *Pten* expression. We monitored the microenvironment changes in the outer one-third of four mice ears, including two 4-OHT drug-induced mice as experimental group and two without drug induction as the control group. **Figure 1** shows the schematic diagram of the animal experiment timeline. MCOCT images were scanned at week 0, followed by two consecutive weeks of 4-OHT induction. Tissue sections were taken at week 22 after the death of the induction and control groups of mice. Skin tissues were fixed overnight in 10% neutral buffered formalin at 4°C and then transferred to 70% ethanol before being processed and embedded in paraffin. Paraffin-embedded specimens were cut into 5-μm sections and stained with

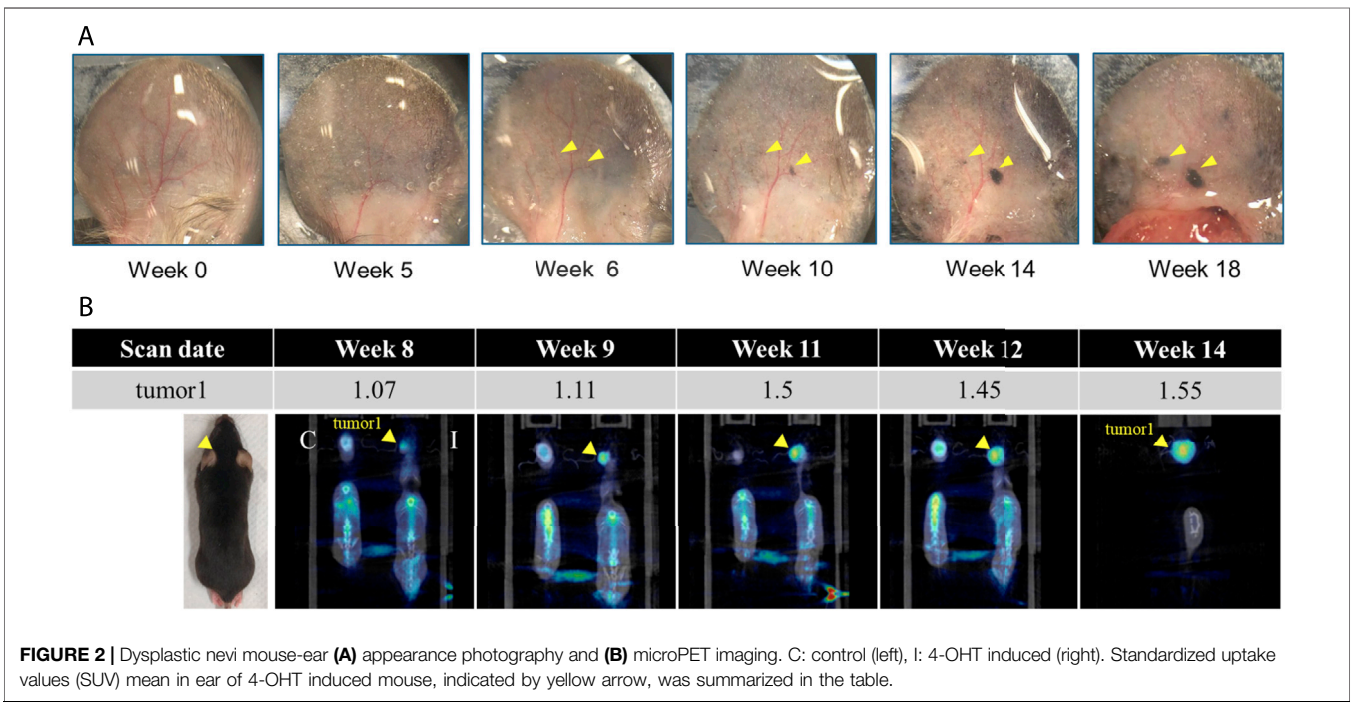

FIGURE 2 | Dysplastic nevi mouse-ear **(A)** appearance photography and **(B)** microPET imaging. C: control (left), I: 4-OHT induced (right). Standardized uptake values (SUV) mean in ear of 4-OHT induced mouse, indicated by yellow arrow, was summarized in the table.

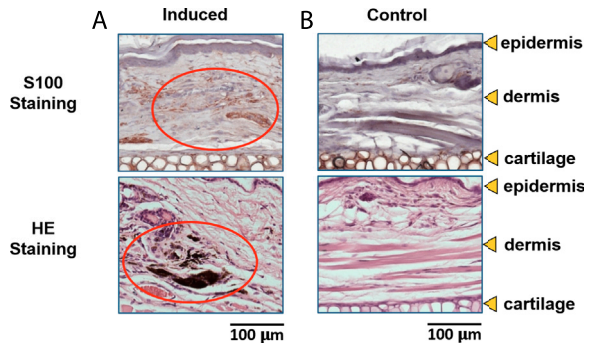

FIGURE 3 | H&E and S100-stained section of **(A)** dysplastic nevus mice at week 22, and **(B)** control mouse at week 22.

hematoxylin and eosin (H&E) and anti-S100 antibodies. Micro-PET imaging was performed at 8–14 weeks of the experimental period. The uptake of 18fluorodeoxyglucose (18 F-FDG) into cancer cells, which have a higher demand for glucose than noncancer cells, can be detected using micro-PET. Within 0–18 weeks of the experimental period, skin appearance (**Figure 1B**), subcutaneous vessels (**Figure 1C**), and (**Figure 1D**) OCT maximum intensity projection (MIP) imaging were taken. The blue part of **Figure 1D** shows the location of the lymphatic vessels. **Figure 1E** is the thickness map where pseudo color represents the distance between the corneum stratum and the articular cartilage in each two-dimension cross-sectional OCT image.

RESULTS

Figure 2 shows a representative dysplastic nevi mouse-ear appearance photography 1) and microPET imaging 2). We found that 4-OHT induced dysplastic nevi mice showed nevi in their ears from week 5 to week 6, and the number of nevi increased with the increase of weeks, and a more prominent black spot appeared in the ear of mice at week 10, as shown in **Figure 2A**, indicated by yellow arrows. Therefore, based on the changes in the skin appearance of mice, we suspect that weeks 5-6 are the weeks when nevi are produced after drug-induced nevi in dysplastic nevi mice, and weeks 8-9 are the critical weeks when nevi gradually turn into melanoma. To verify the transformation of dysplastic nevi into malignant melanoma, microPET imaging was performed starting from week 8. **Figure 2B** shows the 18 F-FDG amassments in one representative 4-OHT induced mice in week 8, week 9, and weeks 11, 12, 14. Compared with the control group (C: left figure in b), a tumor was found in the induced group (I: right figure in b).

Figure 3 is the H&E and S100-stained section of dysplastic nevus mice 1) and control mouse 2) at week 22. Compared with dysplastic nevus mice and control mice, staining with S100 antibody showed an increased number of melanocytes in dysplastic nevus mice, indicated by red circle. H&E-stained section of dysplastic nevus mice also exhibits accumulation of

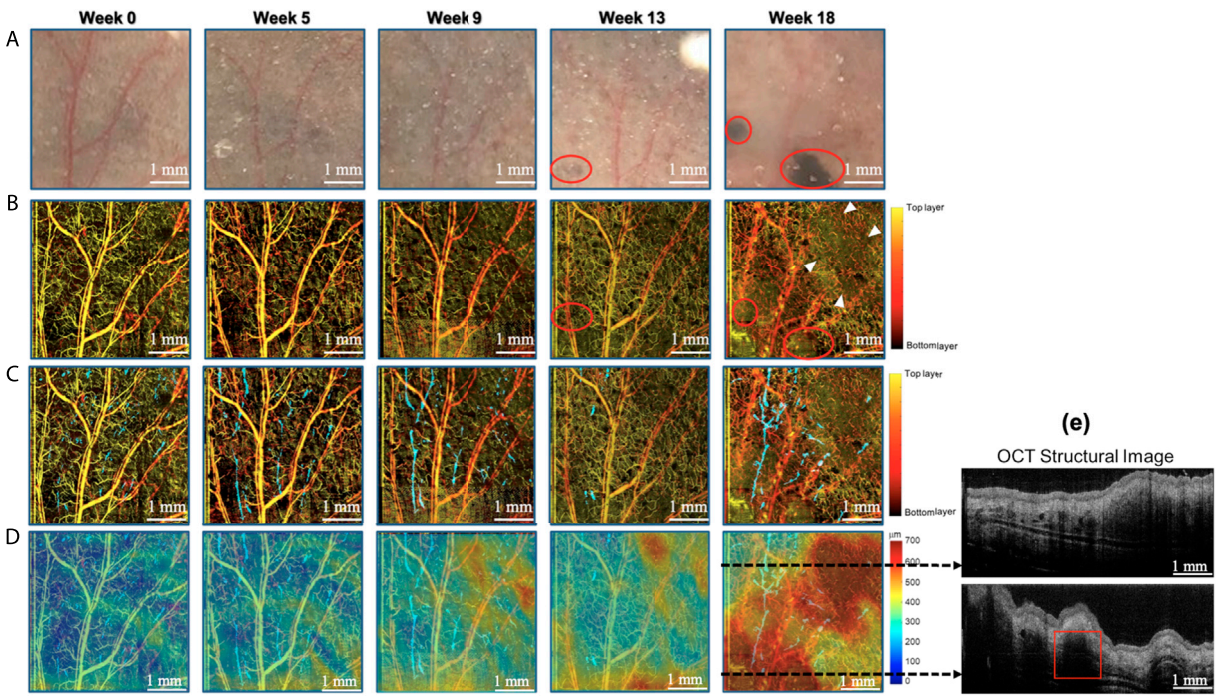

FIGURE 4 | Longitudinal tracking of blood vessels, lymphatic vessels using MFOCT in a dysplastic nevi mouse ear. **(A)** Photograph, **(B)** angiography, **(C)** combined angiography and lymphangiography, and **(D)** combined angiography, lymphangiography, and thickness map. **(E)** The cross-section OCT image shows the anatomy structure at the dotted line in **(D)**.

melanin. Here histology confirms the melanoma appearance at the endpoint (week 22).

We imaged subcutaneous vessels before 4-OHT induction (week 0) and during 18 consecutive weeks after induction. **Figure 4** shows 1) photographs, 2) depth-coded vascular imaging, 3) combined vascular imaging and lymphatic vessel imaging, and 4) combined vascular imaging, lymphatic vessel imaging, and thickness maps at week 0, week 5, week 9, week 13 and week 18. Moles are detectable starting at week five and become evident at week 13, which is indicated by the red circle on the photograph. At each imaging, the lymphatic vessels developed more distinctly over time as the size of the nevus continued to grow. On the other hand, the vascular pattern becomes irregular and disorganized, and at weeks 13 and 18, the capillaries increase in density and are distinguishable from the vessels of normal tissue at week 0. After the growth of dysplastic nevi, larger vessels remained relatively unchanged compared to smaller capillaries. Structural changes are noted in the angiogram at week 18 and are indicated by white arrows. The thickness of the ear varies from 200 to 400 μm at week 0 and finally thickens from 400 to 700 μm at week 18. At week 18, the thickness of the ear is not uniformly distributed throughout the imaging area, with some areas thicker than others (~ 700 μm). **Figure 4E** demonstrates the 2D cross-sectional OCT images where a red square indicates suspicious melanoma sites at week 18. From the superimposition of angiography and lymphography with the thickness maps at week 18, the increase in capillaries of the fragmented morphology corresponds to areas with thicker thickness and more altered surrounding lymphatic vessels. The above results of microvascular and microstructural changes observed at 18 weeks of *in vivo* follow-up suggest that it is possible to see a progression from dysplasia to melanoma using MCOCT.

DISCUSSION AND SUMMARY

The current methods for detecting melanoma in the skin include visualization (ABCD law), dermoscopy, and pathological biopsy. However, these methods still have several drawbacks, as the visualization can only be used as a preliminary observation, and it is based on the subjective judgment of the doctor to distinguish the lesion from the malignancy, which lacks objectivity and accuracy. Pathological biopsy is the best way to determine whether a melanoma is malignant or not [35], but it has limitations such as the inability to make quantitative and continuous observations and being performed on suspicious but still benign lesion [36]. Although the dermoscopy is a non-invasive method, it still lacks the ability to quantify and objectively diagnose the lesions. In addition, in medical diagnosis, not only the structural characteristics are used as a criterion, but also the function of the tissue is often observed. This is because functional changes usually occur earlier than structural changes, which may be changes in blood flow, collagen fiber content, water content, etc. in the diagnosis of skin diseases. Therefore, more and more non-invasive imaging modalities are developed to aid in skin disease diagnosis and the decision to biopsy [37, 38].

In this study, dysplastic nevi mice with partial deletion of *Pten* can develop nevi changes or even melanoma if induced with the 4-OHT drug. MCOCT is a label-free imaging technique, and its high resolution and multi-contrast images help study the development of dysplastic nevi at different stages. With MCOCT, we can perform noninvasive scans of dysplastic nevi mice to obtain extensive information on the subcutaneous microenvironment, such as images of blood vessels and lymphatic vessels. In the subcutaneous structural images, we found that the ear thickness changes when the mouse ear appearance of nevi increases or becomes larger (week 9). When dysplastic nevi deteriorate, both the epidermis and dermis thicken, so the subcutaneous structural changes of the ear are an important observation in the progression of dysplastic nevi tumors. In addition, when 4-OHT induced mice showed significant changes in the appearance of nevi at week 9, their lymphatic vessels also showed increased density and enlarged diameter (**Figure 4**). Therefore, we hypothesized that during the progress of dysplastic nevi, if the nevi showed diffusion or hyperplasia, the subcutaneous microstructure would show apparent changes, such as an increase in thickness, increase in the number of lymphatic vessels, and dilatation of the vessel wall. With the progress of time, the epidermis and dermis would be thickened, and vascular fragmentation would occur.

The tumor progression of dysplastic nevi is not yet clear, but it is expected that if MCOCT observes the pattern of changes, the symptoms can be detected earlier, and surgical resection or targeted therapy can be performed earlier to improve the 5-year survival rate of patients. At present, we found some subcutaneous micro-environmental changes during dysplastic nevi carcinogenesis compared to the control group. We also found an increase in lymphatic vessels and dilation of the wall before the appearance of nevi accumulation in the ear. We hope this finding can be applied in the future to improve the accuracy of the diagnosis of dysplastic nevi through the subcutaneous micro-environmental changes observed by MCOCT. Patients can be treated earlier and reduce the possibility of dysplastic nevi turning into melanoma.

DATA AVAILABILITY STATEMENT

The data that support the findings of this study are available from the corresponding author upon reasonable request.

ETHICS STATEMENT

The animal study was reviewed and approved by Institutional Animal Care and Use Committee (IACUC) of National Yang Ming Chiao Tung University.

AUTHOR CONTRIBUTIONS

W-CK: Project administration, supervision, original draft preparation, review, and editing. C-HC: Conceptualization, funding acquisition, and supervision; P-YL and T-YS: Data curation, measurement, and analysis.

FUNDING

This research was supported, in part, by the Ministry of Science and Technology (MOST), Taiwan 110-2112-M-A49A-502 (W-CK); and MOST Taiwan 107-21 2314-B-303-010-MY3 (C-HC).

REFERENCES

1. O'Neill CH, Scoggins CR. *Melanoma. J Surg Oncol* (2019).
2. Bastian BC. The Molecular Pathology of Melanoma: an Integrated Taxonomy of Melanocytic Neoplasia. *Annu Rev Pathol Mech Dis* (2014) 9:239–71. doi:10.1146/annurev-pathol-012513-104658
3. Sung W-W, Chang C-H. Nevi, Dysplastic Nevi, and Melanoma: Molecular and Immune Mechanisms Involving the Progression. *Tzu Chi Med. J.* (2022) 34(1):1-7.
4. Elder DE. Dysplastic Naevi: an Update. *Histopathology* (2010) 56(1):112–20. doi:10.1111/j.1365-2559.2009.03450.x
5. Emmett MS, Symonds KE, Rigby H, Cook MG, Price R, Metcalfe C, et al. Prediction of Melanoma Metastasis by the Shields index Based on Lymphatic Vessel Density. *BMC Cancer* (2010) 10:208. doi:10.1186/1471-2407-10-208
6. Ji R-C, Eshita Y, Kobayashi T, Hidano S, Kamiyama N, Onishi Y. Role of Simvastatin in Tumor Lymphangiogenesis and Lymph Node Metastasis. *Clin Exp Metastasis* (2018) 35(8):785–96. doi:10.1007/s10585-018-9940-8
7. Fankhauser M, Broggi MAS, Potin L, Bordry N, Jeanbart L, Lund AW, et al. Tumor Lymphangiogenesis Promotes T Cell Infiltration and Potentiates Immunotherapy in Melanoma. *Sci Transl Med* (2017) 9(407):1. doi:10.1126/scitranslmed.aal4712
8. Cho WC, Jour G, Aung PP. Role of Angiogenesis in Melanoma Progression: Update on Key Angiogenic Mechanisms and Other Associated Components. *Semin Cancer Biol* (2019) 59:175–86. doi:10.1016/j.semcancer.2019.06.015
9. Zhou Z, Mao W, Li Y, Qi C, He Y. Myricetin Inhibits Breast Tumor Growth and Angiogenesis by Regulating VEGF/VEGFR2 and p38MAPK Signaling Pathways. *Anat Rec (Hoboken)* (2019) 302(12):2186–92. doi:10.1002/ar.24222
10. Castet F, Garcia-Mulero S, Sanz-Pamplona R, Cuellar A, Casanovas O, Caminal JM, et al. Uveal Melanoma, Angiogenesis and Immunotherapy, Is There Any Hope? *Cancers (Basel)* (2019) 11(6). doi:10.3390/cancers11060834
11. Fontaine R, Weltzien FA. Labeling of Blood Vessels in the Teleost Brain and Pituitary Using Cardiac Perfusion with a DiI-Fixative. *J Vis Exp* (2019) 148:1. doi:10.3791/59768
12. Aki R, Amoh Y, Bouvet M, Katsuoka K, Hoffman RM. Color-coded Fluorescence Imaging of Lymph-Node Metastasis, Angiogenesis, and its Drug-Induced Inhibition. *J Cel Biochem.* (2014) 115(3):457–63. doi:10.1002/jcb.24677
13. Sharma KS, Lim P, Brotherston MT. Excision versus Incision Biopsy in the Management of Malignant Melanoma. *J Dermatol Treat* (2016) 27(1):88–90. doi:10.3109/09546634.2015.1034083
14. Theotoka D, Morkin MI, Galor A, Karp CL. Update on Diagnosis and Management of Conjunctival Papilloma. *Eye Vis* (2019) 6:18. doi:10.1186/s40662-019-0142-5
15. Mailankody P, Lenka A, Pal PK. The Role of Optical Coherence Tomography in Parkinsonism: A Critical Review. *J Neurol Sci* (2019) 403:67–74. doi:10.1016/j.jns.2019.06.009
16. Dingerkus VLS, Munk MR, Brinkmann MP, Freiberg FJ, Heussen FMA, Kinzl S, et al. Optical Coherence Tomography Angiography (OCTA) as a New Diagnostic Tool in Uveitis. *J Ophthal Inflamm Infect* (2019) 9(1):10. doi:10.1186/s12348-019-0176-9
17. Abdlaty R, Hayward J, Farrell T, Fang Q. Skin Erythema and Pigmentation: a Review of Optical Assessment Techniques. *Photodiagnosis Photodynamic Ther* (2021) 33:102127. doi:10.1016/j.pdpdt.2020.102127
18. Kardynal A, Olszewska M. Modern Non-invasive Diagnostic Techniques in the Detection of Early Cutaneous Melanoma. *J Dermatol Case Rep* (2014) 8(1):1–8. doi:10.3315/jdcr.2014.1161
19. Leon R, Martinez-Vega B, Fabelo H, Ortega S, Melian V, Castaño I, et al. Non-Invasive Skin Cancer Diagnosis Using Hyperspectral Imaging for In-Situ Clinical Support. *J Clin Med* (2020) 9(6). doi:10.3390/jcm9061662
20. Zhang Y, Moy AJ, Feng X, Nguyen HTM, Reichenberg JS, Markey MK, et al. Physiological Model Using Diffuse Reflectance Spectroscopy for Nonmelanoma Skin Cancer Diagnosis. *J Biophotonics* (2019) 12:e201900154. doi:10.1002/jbio.201900154
21. Dinnes J, Bamber J, Chuchu N, Bayliss SE, Takwoingi Y, Davenport C, et al. High-frequency Ultrasound for Diagnosing Skin Cancer in Adults. *Cochrane Database Syst Rev* (2018) 12:CD013188. doi:10.1002/14651858.CD013188
22. Edwards SJ, Osei-Assibey G, Patalay R, Wakefield V, Karner C. Diagnostic Accuracy of Reflectance Confocal Microscopy Using VivaScope for Detecting and Monitoring Skin Lesions: a Systematic Review. *Clin Exp Dermatol* (2017) 42:266–75. doi:10.1111/ced.13055
23. Liang K, Ahsen OO, Murphy A, Zhang J, Nguyen TH, Potsaid B, et al. Tethered capsule en face optical coherence tomography for imaging Barrett's oesophagus in unsedated patients. *BMJ Open Gastroenterol* (2020) 7(1):e000444. doi:10.1136/bmjgast-2020-000444
24. Abdlaty R, Doerwald-Munoz L, Farrell TJ, Hayward JE, Fang Q. Hyperspectral Imaging Assessment for Radiotherapy Induced Skin-Erythema: Pilot Study. *Photodiagnosis Photodynamic Ther* (2021) 33:102195. doi:10.1016/j.pdpdt.2021.102195
25. Miller DT, Kurokawa K. Cellular-Scale Imaging of Transparent Retinal Structures and Processes Using Adaptive Optics Optical Coherence Tomography. *Annu Rev Vis Sci* (2020) 6(1):115–48. doi:10.1146/annurev-vision-030320-041255
26. Lai P-Y, Shih T-Y, Chang Y-H, Chou Y-S, Wu T-H, Su Y-Y, et al. *In Vivo* Longitudinal Tracking of Lymphangiogenesis and Angiogenesis in Cutaneous Melanoma Mouse Model Using Multifunctional Optical Coherence Tomography. *JID Innov* (2021) 1:100010. doi:10.1016/j.xjidi.2021.100010, *In*
27. Shimada Y, Yoshiyama M, Tagami J, Sumi Y. Evaluation of Dental Caries, Tooth Crack, and Age-Related Changes in Tooth Structure Using Optical Coherence Tomography. *Jpn Dental Sci Rev* (2020) 56(1):109–18. doi:10.1016/j.jdsr.2020.08.001
28. Syu J-P, Buddhakosai W, Chen S-J, Ke C-C, Chiou S-H, Kuo W-C. Supercontinuum Source-Based Multi-Contrast Optical Coherence Tomography for Rat Retina Imaging. *Biomed Opt Express* (2018) 9(12):6132–44. doi:10.1364/boe.9.006132
29. Chen PH, Lee HY, Chen YF, Yeh YC, Chang KW, Hou MC, et al. Detection of Oral Dysplastic and Early Cancerous Lesions by Polarization-Sensitive Optical

Coherence Tomography. *Cancers (Basel)* (2020) 12(9):1. doi:10.3390/cancers12092376
30. Chen P-H, Chen Y-J, Chen Y-F, Yeh Y-C, Chang K-W, Hou M-C, et al. Quantification of Structural and Microvascular Changes for Diagnosing Early-Stage Oral Cancer. *Biomed Opt Express* (2020) 11(3):1244–56. doi:10.1364/boe.384608
31. Kuo W-C, Kuo Y-M, Wen S-Y. Quantitative and Rapid Estimations of Human Subsurface Skin Mass Using Ultra-high-resolution Spectral Domain Optical Coherence Tomography. *J Biophoton* (2016) 9(4):343–50. doi:10.1002/jbio.201400153
32. Lai P-Y, Chang C-H, Su H-R, Kuo W-C. Lymphatic Vessel Segmentation in Optical Coherence Tomography by Adding U-Net-Based CNN for Artifact Minimization. *Biomed Opt Express* (2020) 11(5):2679–93. doi:10.1364/boe.389373
33. Wang RK. Optical Microangiography: A Label-free 3-D Imaging Technology to Visualize and Quantify Blood Circulations within Tissue Beds *In Vivo*. *IEEE J Select Top Quan Electron.* (2010) 16(3):545–54. doi:10.1109/jstqe.2009.2033609
34. Dankort D, Curley DP, Cartlidge RA, Nelson B, Karnezis AN, Damsky Jr WE, et al. BrafV600E Cooperates with Pten Loss to Induce Metastatic Melanoma. *Nat Genet* (2009) 41(5):544–52. doi:10.1038/ng.356
35. Kilic A, Kilic A, Kivanc AE, Sisik A. Biopsy Techniques for Skin Disease and Skin Cancer: A New Approach. *J Cutan Aesthet Surg* (2020) 13(3):251–4. doi:10.4103/JCAS.JCAS_173_19
36. Wilson RL, Yentzer BA, Isom SP, Feldman SR, Fleischer Jr AB. How Good Are US Dermatologists at Discriminating Skin Cancers? A Number-Needed-To-Treat Analysis. *J Dermatol Treat* (2011) 23:65–9. doi:10.3109/09546634.2010.512951
37. Abdlaty R, Doerwald L, Hayward JE, Fang Q. *Spectral Assessment of Radiation Therapy-Induced Skin Erythema* (2020).
38. Borsari S, Pampena R, Lallas A, Kyrgidis A, Moscarella E, Benati E, et al. Clinical Indications for Use of Reflectance Confocal Microscopy for Skin Cancer Diagnosis. *JAMA Dermatol* (2016) 152:1093–8. doi:10.1001/jamadermatol.2016.1188

Conflict of Interest: The authors declare that the research was conducted in the absence of any commercial or financial relationships that could be construed as a potential conflict of interest.

Publisher's Note: All claims expressed in this article are solely those of the authors and do not necessarily represent those of their affiliated organizations, or those of the publisher, the editors and the reviewers. Any product that may be evaluated in this article, orclaim that may be made by its manufacturer, is not guaranteed or endorsed by the publisher.